Effects of Inorganic Salts on the Heterogeneous OH Oxidation of Organic Compounds: Insights from Methylglutaric Acid-Ammonium Sulfate

Hoi Ki Lam[1], Sze Man Shum[1], James F. Davies[2], Mijung Song[3], Andreas Zuend[4], and Man Nin Chan[1,5,*]

[1]Earth System Science Programme, Faculty of Science, The Chinese University of Hong Kong, Hong Kong, China

[2]Department of Chemistry, University of California Riverside, Riverside, CA, USA

[3]Department of Earth and Environmental Sciences, Chonbuk National University, Jeollabuk-do, Republic of Korea

[4]Department of Atmospheric and Oceanic Sciences, McGill University, Montreal, Québec, Canada

[5]The Institute of Environment, Energy, and Sustainability, The Chinese University of Hong Kong, Hong Kong, China

Corresponding author: mnchan@cuhk.edu.hk

Abstract

Atmospheric particles, consisting of inorganic salts, organic compounds and a varying amount of water, can continuously undergo heterogeneous oxidation initiated by gas-phase oxidants at the particle surface, changing the composition and properties of particles over time. To date, most studies focus on the chemical evolution of pure organic particles upon oxidation. To gain more fundamental insights into the effects of inorganic salts on the heterogeneous kinetics and chemistry of organic compounds, we investigate the heterogeneous OH oxidation of 3-methylglutaric acid (3-MGA) particles and particles containing both 3-MGA and ammonium sulfate (AS) in an organic-to-inorganic mass ratio of 2 in an aerosol flow tube reactor at a high relative humidity of 85.0 %. The molecular information of the particles before and after OH oxidation is obtained using the Direct Analysis in Real Time (DART), a soft atmospheric pressure ionization source, coupled to a high-resolution mass spectrometer. Optical

microscopy measurements reveal that 3-MGA-AS particles are in a single liquid phase prior to oxidation at high relative humidity. Particle mass spectra show that C_6 hydroxyl and C_6 ketone functionalization products are the major products formed upon OH oxidation in the absence and presence of AS, suggesting that the dissolved salt does not significantly affect reaction pathways. The

5   dominance of C_6 hydroxyl products over C_6 ketone products could be explained by the intermolecular hydrogen abstraction by tertiary alkoxy radicals formed at the methyl-substituted tertiary carbon site. On the other hand, kinetic measurements show that the effective OH uptake coefficient, γ_{eff}, for 3-MGA-AS particles (0.99 ± 0.05) is smaller than that for 3-MGA particles (2.41 ± 0.13) by about a factor of ~2.4. A smaller reactivity observed in 3-MGA-AS particles might be attributed to a higher

10   surface concentration of water molecules, and the presence of ammonium and sulfate ions, which are chemically inert to OH radicals, at the particle surface. This could lower the collision probability between the 3-MGA and OH radicals, resulting in a smaller overall reaction rate. Our results suggest that inorganic salts likely alter the overall heterogeneous reactivity of organic compounds with gas-phase OH radicals rather than reaction mechanisms in well-mixed aqueous organic-inorganic particles.

1. Introduction

Atmospheric particles are chemically complex and are comprised of a large variety of organic compounds, inorganic salts and water. Organic compounds contribute a significant mass fraction (20-90 %) of atmospheric particles (Kanakidou et al., 2005; Zhang et al., 2007; Jimenez et al., 2009).

20   Laboratory and modeling studies have revealed that organic compounds present at or near the particle surface can be efficiently oxidized by gas-phase oxidants such as hydroxyl (OH) radicals, ozone (O_3) and nitrate radicals (Rudich et al., 2007; George and Abbatt, 2010; Kroll et al., 2015; Estillore et al., 2016; Chapleski et al., 2016). The effective OH uptake coefficient, γ_{eff}, defined as the fraction of OH collisions with organic molecules that yields a reaction of a target organic molecule, has been

25   commonly used to describe the kinetics and reported for a variety of pure organic compounds. The γ_{eff} in general has a value of ≥ 0.1 and even ≥ 1, indicating the occurrence of secondary chemistry (e.g.

chain reactions induced by the hydrogen abstraction of organic molecules by alkoxy radicals) (Richards-Henderson et al., 2015). These heterogenous oxidative processes can continuously alter the surface and bulk composition of the particles (Slade and Knopf, 2013; Li et al., 2018), and thus modify particle properties such as light extinction, hygroscopicity and cloud condensation nuclei activity

5   (George et al., 2007; Lambe et al., 2007, 2009; Cappa et al., 2011).

While the transformation of pure organic particles has become more reasonably understood, the chemical transformation of organic particles in the presence of dissolved inorganic salts is largely unclear. Only a few laboratory studies have investigated the heterogeneous oxidation of organic-

10   inorganic particles (McNeill et al., 2007, 2008; Dennis-Smither et al., 2012). In those studies, hydrophobic organic compounds (e.g. oleic acid and palmitic acid) have been chosen as model compounds. Due to the hydrophobic nature of these compounds, the particles tend to be phase-separated with a thin organic layer on the surface of aqueous inorganic core (e.g. aqueous sodium chloride or ammonium sulfate (AS) phases). For these phase-separated particles, the molecular

15   structure and orientation of organic molecules at the particle surface are observed to alter the reactive uptake of gas-phase oxidants such as O_3 and OH radicals. The reaction products formed from the ozonolysis of oleic acid-AS particles are very similar to those found in pure oleic acid particles (McNeill et al., 2007). These observations are consistent with the hypothesis that a thin organic layer effectively shields the aqueous inorganic core from being oxidized at the particle surface.

To date, there are still uncertainties on how salts affect the heterogeneous reactivity of organic compounds, in particular, the more oxygenated ones which exhibit moderate to high solubility in water. In this work, experiments were conducted to investigate the evolution of molecular composition of 3-methylglutaric acid (3-MGA) particles and particles containing 3-MGA and AS in an organic-to-

25   inorganic mass ratio (water-free) (OIR) of 2 upon heterogeneous OH oxidation at a relative humidity (RH) of 85.0 % using an aerosol flow tube reactor coupled to the Direct Analysis in Real Time (DART)

mass spectrometry. 3-MGA is chosen as a model compound for methyl-substituted dicarboxylic acids (**Table 1**), while AS is chosen as the model inorganic salt. The OIR of 2 used in this work is in the range of OIR commonly observed in atmospheric particles (Jimenez et al., 2009). The model system allows us to gain more insights into the physics and chemistry of heterogeneous reactions. The physical

5   state of the particle is known to be a key factor in controlling the heterogeneous reactivity (Renbaum and Smith, 2009; Shiraiwa et al., 2011; Chan et al., 2014; Slade and Knopf, 2014; Fan et al., 2015; Marshall et al., 2018). Recent laboratory and modeling studies have shown that in addition to deliquescence and efflorescence, particles containing organic compounds and inorganic salts can undergo phase separation, depending on the particle composition and environmental conditions such

10   as RH and temperature (Ciobanu et al., 2009; Reid et al., 2011; Song et al., 2012ab; Zuend and Seinfeld, 2012; Qiu and Molinero, 2015; Stewart, et al., 2015; You and Bertram, 2015; Freedman, 2017; Losey et al., 2018). Since whether particles are well-mixed or phase-separated governs the surface composition of particles and thus the heterogeneous reactivity, the phase separation behavior of 3-MGA-AS particles was investigated using an aerosol flow cell coupled to an optical microscope. By

15   assessing the molecular transformation of 3-MGA and 3-MGA-AS particles upon oxidation together with phase separation data obtained from optical microscopy measurements, the effects of AS on the heterogeneous OH kinetics and chemistry of 3-MGA are examined. More recently, we have measured the heterogeneous OH reactivity of pure 2-MGA particles, a structural isomer of 3-MGA (Chim et al., 2017a). Given their similar structures, the results of this work together with 2-MGA data might provide

20   some new aspects on how dissolved inorganic salts would alter the heterogeneous kinetics and chemistry of methyl substituted dicarboxylic acids.

2. Experimental Methods

2.1 Heterogeneous OH oxidation of 3-MGA and 3-MGA-AS particles

25   The OH-initiated heterogeneous oxidation of 3-MGA and 3-MGA-AS particles were performed in an aerosol flow tube reactor at 85.0 % RH. Details of the experimental methods have been described

elsewhere (Chim et al., 2017ab). In brief, an aqueous solution of 3-MGA or 3-MGA-AS in an OIR of

2 was atomized using a TSI atomizer to generate aqueous droplets. The particle stream was then mixed

with O_3, oxygen (O_2), dry nitrogen (N_2), humidified N_2 and hexane, and was introduced into the reactor.

The RH within the reactor was controlled by varying the dry N_2 to humidified N_2 ratio. A water jacket

5   was used to maintain a constant temperature of 20 °C inside the reactor. Inside the reactor, gas-phase

OH radicals were generated via the photolysis of O_3 using UV lamps at 254 nm. The processes can be

described by the following reactions:

$$O_3 \rightarrow O(^1D) + O_2 \tag{R1}$$

$$O(^1D) + H_2O \rightarrow 2\ OH \tag{R2}$$

10   The gas-phase concentration of OH radicals was controlled by varying the O_3 concentration introduced

to the reactor and was determined by measuring the decay of hexane, a gas-phase tracer of OH radicals,

using a gas chromatograph coupled with a flame ionization detector (GC-FID). The OH exposure, a

quantity defined as the product of OH concentration and particle residence time, can be determined by

the following equation (Smith et al., 2009):

15    $$OH\ exposure = -\ \frac{\ln\left(\frac{[Hex]}{[Hex]_0}\right)}{k_{Hex}} = \int_o^t [OH]dt \tag{Eqn. 1}$$

where k_{Hex} is the rate constant for the reaction of OH radicals with hexane (5.2×10^{-12} cm^3 molecule^{-1}

s^{-1}), $[Hex]_0$ is the initial hexane concentration entering the reactor, and $[Hex]$ is the concentration of

hexane leaving the reactor. The OH exposure was varied from 0 to a maximum of 4.06×10^{11} molecules

cm^{-3} s in 3-MGA experiments and was varied from 0 to a maximum of 3.84×10^{11} molecules cm^{-3} s in

20   3-MGA-AS experiments. The oxidation levels are equivalent to about 3 days in the atmosphere under

a moderate to high level of OH concentration (1.5×10^6 molecules cm^{-3}). Upon exiting the reactor, the

particle stream then passed through an annular Carulite catalyst denuder for O_3 removal and an

activated charcoal denuder for the removal of organic gas-phase species remaining in the stream.

Hence, only particle-phase reaction products were analyzed. Size distribution of the particles was

25   determined by sampling a small portion of the particle stream using a scanning mobility particle sizer

(SMPS, TSI). The remaining flow was directed to a heater at 250–300 ℃ to fully vaporize the particles. 3-MGA and 3-MGA-AS particles were confirmed to be fully vaporized upon heating at 250 ˚C or above by measuring the size distribution of the particles leaving the heater with the SMPS in separate experiments. The resulting gas-phase species were then directed to an ionization region, a narrow open

5   space between the DART ionization source (IonSense: DART SVP), and the inlet of the high-resolution mass spectrometer (ThermoFisher, Q Exactive Orbitrap) (Chan et al., 2013; Nah et al., 2013).

Details of the DART operation have been described in the work of Cody et al. (2005). The DART ionization source was operated in negative ionization mode with helium (He) as the ionizing gas. The

10   formation of gas-phase ions in the ionization region can be described by below (Cody, 2009):

$$e^- + O_2(g) \rightarrow O_2^-(g) \qquad\qquad (R3)$$

$$O_2^-(g) + M(g) \rightarrow [M-H]^-(g) + HO_2(g) \quad (R4)$$
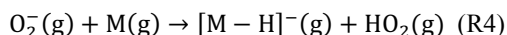
Atmospheric O_2 molecules abstract the electrons (e^-) produced by the Penning ionization of metastable He in the DART ionization source to form anionic oxygen ions (O_2^-) which then react with the gas-

15   phase species (M) to form deprotonated molecular ions ($[M-H]^-$) by proton abstraction. Previous studies have shown that the acidic proton of the carboxyl group can be abstracted by the O_2^- ions to generate the $[M-H]^-$, which was observed dominantly in the mass spectra (Cheng et al., 2015; Chim et al., 2017ab). In this work, it is likely that proton abstraction from the carboxyl group of 3-MGA and its reaction products occurred to produce the $[M-H]^-$. These ions were sampled by the high-resolution

20   mass spectrometer. Mass spectra, over a scan range from *m/z* 70–400 at a mass resolution of about 140000, were collected. The mass spectra were analyzed using the Xcalibur software (Xcalibur Software, Inc., Herndon, VA, USA). Two control experiments were conducted: one in the presence of O_3 without the UV light and another one in the absence of O_3 with the UV light on. No compositional changes were observed for 3-MGA and 3-MGA-AS particles in both control experiments, indicating

25   that the reaction of 3-MGA with O_3 is insignificant and that 3-MGA is not likely to be photolyzed.

Optical microscopy measurements have been carried out (**Figure S1,** *supplementary material*) and show that 3-MGA-AS particles are in a single liquid phase prior to oxidation at 85.0 % RH as the particles become phase-separated when the RH is below the separation RH (SRH = 72.7–73.6 %) (**Figure S2,** *supplementary material*). Details of the optical microscopy measurements have been given

5   in the *Supplementary Material*. Since the particles were always exposed to high humidity and the experiments were carried out at 85.0 % RH, which is higher than the SRH, 3-MGA-AS particles are likely to be single-phase liquid droplets prior to oxidation.

3 Results and Discussion

10   **3.1 Particle mass spectra of 3-MGA and 3-MGA-AS before and after OH oxidation**

Figure 1 shows the mass spectra of 3-MGA and 3-MGA-AS before and after OH oxidation at 85.0 % RH, respectively. For 3-MGA, a dominant peak is observed before oxidation at m/z = 145 which corresponds to the deprotonated molecular ion of 3-MGA ($C_6H_9O_4^-$). After oxidation, two major product peaks evolve, corresponding to two C_6 functionalization products (C_6 hydroxyl products

15   ($C_6H_{10}O_5$) and C_6 ketone products ($C_6H_8O_5$)). A few minor product peaks, such as $C_4H_5O_3^-$, $C_5H_5O_3^-$, $C_5H_7O_3^-$, $C_5H_7O_4^-$ and $C_5H_7O_5^-$, are also observed. Each of these peaks contributes less than 2.5 % of the total ion signal at the maximum OH exposure. The mass spectra of 3-MGA-AS particles in OIR = 2 are very similar to those of 3-MGA particles, except for the two inorganic sulfate peaks that originate from dissolved AS. Before oxidation (**Figure 1**), three peaks at m/z = 97, m/z = 145 and m/z = 195 are

20   observed, corresponding to the bisulfate ion (HSO_4^-), the deprotonated molecular ion of 3-MGA and $H_3S_2O_8^-$, respectively. One possibility is that HSO_4^- is likely the dissolved ion from aqueous AS that became acidified by the evaporative loss of ammonia (NH_3) into gas phase and can be detected via direct ionization in the negative ion mode (Hajslova et al., 2011). HSO_4^- has been detected when aqueous AS particles are ionized by the DART ionization source as well as when being a reaction

25   product formed in the heterogeneous OH oxidation of sodium methyl sulfate, sodium ethyl sulfate and methanesulfonic acid particles (Kwong et al., 2018ab). However, we do not have a clear explanation

for the formation of $H_3S_2O_8^-$ which is likely an adduct of HSO_4^- and H_2SO_4. After oxidation, the deprotonated ions of C_6 hydroxyl ($C_6H_9O_5^-$) and C_6 ketone products ($C_6H_7O_5^-$) are observed in addition to the unreacted 3-MGA. Some small product peaks are detected ($C_4H_5O_3^-$, $C_5H_5O_3^-$, $C_5H_7O_3^-$, $C_5H_7O_4^-$ and $C_5H_7O_5^-$); with each contributing less than 2.5 % of the total ion signal.

As shown in **Figure 2**, the chemical evolution in the composition of 3-MGA and 3-MGA-AS particles upon oxidation are very similar. At the maximum OH exposure, the C_6 hydroxyl products are the most abundant species, which accounts for 38.0−48.2 % of the total organic ion signal, followed by unreacted 3-MGA (37.3−47.9 %), and the C_6 ketone products (7.3−7.6 %). For 3-MGA-AS, the

10 intensities of HSO_4^- and $H_3S_2O_8^-$ remain about the same before and after OH oxidation (**Figure S3,** *supplementary material*). This could be attributed to the fact that dissolved AS does not react effectively with gas-phase OH radicals at the particle surface (George and Abbatt, 2010). In general, the same reaction products are observed for both 3-MGA and 3-MGA-AS particles after oxidation, suggesting that AS does not significantly affect the reaction pathways.

3.3 Oxidative Kinetics of 3-MGA and 3-MGA-AS

The normalized parent decay in 3-MGA and 3-MGA-AS particles as a function of OH exposure at 85.0 % RH is shown in **Figure 3**. For both systems, the OH-initiated decay of 3-MGA follows an exponential trend and can be fit with an exponential function to obtain an effective second order OH

20 reaction rate constant (k):

$$\ln \frac{I}{I_0} = -k \, [\text{OH}] \, t \qquad \text{(Eqn. 2)}$$

where I_0 is the ion signals of 3-MGA before oxidation, I is the ion signals of 3-MGA at a given OH exposure, [OH] is the gas-phase concentration of OH radical and t is the reaction time. The fitted value of k for the 3-MGA and 3-MGA-AS are $(3.26 \pm 0.065) \times 10^{-12}$ cm^3 molecule^{-1} s^{-1} and (2.72 ± 0.064)

25 $\times 10^{-12}$ cm^3 molecule^{-1} s^{-1}, respectively. Using the fitted k value, the effective OH uptake coefficient, γ_{eff}, defined as the fraction of OH collisions with particles that yields a reaction, can be computed by the following equation (Davies and Wilson, 2015):

$$\gamma_{\text{eff}} = \frac{2\,\rho_0 D_0\,mfs\,N_A\,k}{3\,M_w\,\overline{c_{OH}}}$$ (Eqn. 3)

where ρ_0 is the density of particle, D_0 is the particle diameter, mfs is the mass fraction of 3-MGA in the particle, M_w is the molecular weight of 3-MGA, N_A is Avogadro's number, and $\overline{c_{OH}}$ is the mean speed of gas-phase OH radicals. Before oxidation, the diameter of 3-MGA and 3-MGA-AS particles

5   were measured to be 203.0 nm and 200.8 nm, respectively. The mfs values were obtained from equilibrium composition calculations using the Aerosol Inorganic-Organic Mixtures Functional groups Activity Coefficients (AIOMFAC) model available online (https://aiomfac.lab.mcgill.ca) (**Table 1**) (Zuend et al., 2008; Zuend et al., 2011). Based on the composition (i.e. mfs), the densities of 3-MGA and 3-MGA-AS particles were estimated using the volume additivity rule with the density of water, 3-

10   MGA and AS (Chim et al., 2017a). Using Eqn. 3, the γ_{eff} for 3-MGA and 3-MGA-AS are calculated to be 2.41 ± 0.13 and 0.99 ± 0.05, respectively. The values of γ_{eff} for 3-MGA-AS particles is smaller than that of 3-MGA particles by about 59 %. One possible explanation is that the mass fraction of 3-MGA in 3-MGA-AS particles (mfs = 0.344) is smaller than that in 3-MGA particles (mfs = 0.707) at 85.0 % RH before oxidation (**Table 1**), likely resulted from the presence of AS and the concomitant increase

15   in particle hygroscopicity. A simple analysis shows that the surface coverage of 3-MGA in 3-MGA particles and 3-MGA-AS particles are roughly estimated to be 51.4% and 21.6%, respectively (*Supplementary material*). A smaller surface concentration of 3-MGA in 3-MGA-AS particles might reduce the collision probability between 3-MGA and gas-phase OH radicals at the air-particle interface and thus lower the overall reactivity, as compared to 3-MGA particles.

A similar result has also been observed for the OH oxidation with methanesulfonic acid (MSA) reported in the literature. Mungall et al. (2017) have investigated the heterogeneous OH oxidation of MSA-AS particles with a mass fraction of MSA = 0.16 at 75 % RH. The γ_{eff} was reported to be 0.05 ± 0.03, which is smaller than that of pure MSA particles (γ_{eff} = 0.45 ± 0.14) measured at a slightly higher

25   RH (90 %) (Kwong et al., 2018b). The results obtained in this work and in the literature suggest that

for a given RH, inorganic salts (e.g. AS) might lower the heterogeneous reactivity of organic compounds toward gas-phase OH radicals due to the smaller surface concentration of 3-MGA resulting from the presence of AS and concomitant increase in water uptake. It acknowledges that ammonium (NH_4^+) and sulfate (SO_4^{2-}) ions, which are chemically inert to OH radicals, present at or near the

5   surface could lower the overall reaction rates by reducing the surface concentration of organic compounds. However, the additional effects of NH_4^+ and SO_4^{2-} ions on the surface activity and configuration of organic molecules, which could play a role in determining the heterogeneous activity, are not yet well understood and warrant further investigations.

10   Kinetic measurements show that γ_{eff} for both 3-MGA and 3-MGA-AS particles are close to or greater than one. This indicates that more than one 3-MGA molecule is reacted away per OH radical collision with the particle surface, suggesting the occurrence of secondary chemistry in the particle phase. In the following sections, reaction mechanisms are tentatively proposed and discussed to explain the formation of major products detected in the particle mass spectra and the reaction pathways likely

15   responsible for the secondary chemistry.

3.4 Reaction Mechanisms

As shown in **Figure 2**, the reaction products observed in 3-MGA and 3-MGA-AS particles are about the same upon oxidation. A generalized reaction scheme is thus proposed for both systems based on

20   well-known particle-phase reactions previously published in the literature (Russell, 1957; Bennett and Summers, 1974; George and Abbatt, 2010). As shown in **Scheme 1,** the OH oxidation with 3-MGA can be initiated by the hydrogen abstraction at three different carbon sites: tertiary backbone carbon site (**Path A),** secondary backbone carbon site (**Path B**) and the primary carbon site of the branched methyl group (**Path C**). Depending on the initial OH reaction site, a variety of reaction products can

25   be formed and broadly classified into two groups: functionalization and fragmentation products.

3.4.1 Functionalization products

At the first oxidation step, a hydrogen atom is abstracted from a 3-MGA molecule by an OH radical, forming an alkyl radical that reacts quickly with an O_2 molecule to form a peroxy radical. The major C_6 hydroxyl ($C_6H_{10}O_5$) and C_6 ketone ($C_6H_8O_5$) products can be generated from the self-reactions of two peroxy radicals through the Russell mechanism (**R1**) and/or Bennett-Summers reactions (**R2**). Alternatively, the self-reactions of two peroxy radicals can form two alkoxy radicals which can then abstract hydrogen atoms from the neighboring organic molecules (**R3**) to form C_6 hydroxyl products or react with O_2 molecules (**R4**) to form C_6 ketone products. However, when the hydrogen abstraction occurs at the tertiary carbon site (**Scheme 1, Path A**), only the C_6 hydroxyl product can be formed because only a hydroxyl group can be added to the tertiary carbon site. Depending on initial reaction site, structural isomers of these C_6 hydroxyl and ketone products are likely formed during oxidation.

3.4.2 Fragmentation products

The fragmentation products can be generated from the decomposition of alkoxy radicals (**R5**). For instance, when the initial hydrogen abstraction occurs at the secondary carbon site (**Scheme 1, Path B**), the decomposition of the secondary alkoxy radical can yield either a C_2 ($C_2H_2O_3$) or a C_5 fragmentation product ($C_5H_8O_3$). On the other hand, a C_4 fragmentation product ($C_4H_6O_3$) can be yielded from the decomposition of the alkoxy radical formed at the tertiary carbon site (**Scheme 1, Path A**) while oxidation at the primary carbon site (**Scheme 1, Path C**) can yield a C_3 fragmentation product ($C_3H_4O_3$). For both 3-MGA and 3-MGA-AS, the ion signal intensity of fragmentation products is small (**Figure 1**). For example, only a small signal of C_4 fragmentation product ($C_4H_6O_3$), which is formed from the oxidation at the tertiary carbon site (**Scheme 1, Path A**), is detected. It contributes less than 2% of the total ion signal at the maximum OH exposure. The observed low abundances of fragmentation products could be explained by their higher volatilities (**Tables S1 and S2,** *supplementary material*) and some (e.g. $C_5H_8O_5$) may be explained by the preference on initial OH reaction site as discussed below. It is noted that for 3-MGA-AS particles, the presence of AS increases

the activity coefficients of fragmentation products in the particle phase based on the thermodynamic model predictions and thus increases their volatilities in general (**Table S3**, *supplementary material*).

3.4.3 Large C_6 hydroxyl-to-C_6 ketone product ratio: Implications for secondary chemistry

5   From the particle composition data, a large C_6 hydroxyl-to-C_6 ketone product ratio is observed. At the maximum OH exposure, the relative abundance of C_6 hydroxyl products is about 5.0–6.6 times that of C_6 ketone products for both 3-MGA and 3-MGA-AS particles. We acknowledge that although the ionization efficiencies are not corrected for these products in this study, the ionization efficiency of C_4 hydroxyl products is found to be about the same or even lower than that of C_4 ketone products during

10   the DART ionization processes (Chan et al., 2014). The abundance of C_6 hydroxyl products might be even larger than that of C_6 ketone products after correcting their ionization efficiencies, supporting the statement above. One possible explanation for the dominance of C_6 hydroxyl products is that the OH abstraction may preferentially occur at the tertiary carbon site (**Scheme 1, Path A**) since the tertiary alkyl radicals are more stable than secondary and primary alkyl radicals (Cheng et al., 2015). Only an

15   addition of a hydroxyl group at the tertiary carbon site is allowed via the alkoxy or peroxy radical reactions.

Another possibility is that the branched methyl group may sterically hinder the two peroxy radicals from arranging into a cyclic tetroxide intermediate, which is essential for the formation of hydroxyl

20   and ketone functionalization products through the Russell and the Bennett-Summers mechanisms (Cheng et al., 2015). Alternatively, alkoxy radicals are more likely formed through the self-reaction of two peroxy radicals and can react with neighboring organic molecules (e.g. unreacted 3-MGA) by intermolecular hydrogen abstraction to form the C_6 hydroxyl products. Furthermore, as proposed by Petters et al. (2004) and Vereecken and Peeters (2009), the strong hydrogen bonding among the two

25   terminal carboxyl groups might lower the decomposition rate of the alkoxy radical. This could increase the competitiveness of the intermolecular hydrogen abstraction by the alkoxy radicals. It is worthwhile

to note that the intermolecular hydrogen abstraction can regenerate an alkyl radical and eventually produce peroxy radicals. These peroxy radicals can react again with other peroxy radicals to regenerate alkoxy radicals. This allows the chain reactions to propagate and increases the overall reactivity (i.e. more than one 3-MGA molecule can be reacted per initial OH collision via secondary chemistry and,

5   thus γ_{eff} is larger than one). Overall, the alkoxy radical chemistry, originating from the OH abstraction at the tertiary carbon site at the first oxidation step (**Scheme 1, Path A**) is likely the important reaction pathway for the OH reactions with 3-MGA.

4. Conclusions and Atmospheric Implications

10   Atmospheric particles can keep colliding with gas-phase oxidants, allowing continuous oxidation to occur at or near the particle surface. To better understand how dissolved inorganic salts affect the heterogeneous chemistry and kinetics of organic compounds with gas-phase OH radicals, we investigated the kinetics, products and mechanisms of particles comprised of 3-MGA and 3-MGA-AS in an OIR of 2 upon heterogeneous OH oxidation at 85.0 % RH. Optical microscopy measurements

15   for the detection of phase separation reveal that 3-MGA-AS particles exhibit a single liquid phase prior to oxidation. Same major reaction products are formed as a result of heterogenous OH oxidation with both 3-MGA and 3-MGA-AS particles. These data suggest that the presence of aqueous AS does not significantly affect the formation pathways of major reaction products. On the other hand, in the presence of AS, the heterogeneous reactivity of 3-MGA toward gas-phase OH radicals is slower in 3-

20   MGA-AS particles compared to that in 3-MGA particles. It is likely attributed to a lower concentration of 3-MGA at the surface of 3-MGA-AS particles relative to 3-MGA particles, reducing the collision probability between 3-MGA and gas-phase OH radicals. The results from this work and the literature suggest that the presence of dissolved salts could reduce the overall heterogeneous reactivity of organic compounds with gas-phase OH radicals at the surface by lowering the surface concentration of organic

25   compounds at a given RH and temperature. Until recently, the kinetic parameters (e.g. γ_{eff}) reported in the literature were mostly measured based on experiments with salt-free organic particles. The

chemical lifetime of organic compounds or chemical tracers against heterogeneous OH reaction in the atmosphere could be longer than expected when the salts are present. Further investigations on how the amount and types of inorganic salts alter heterogeneous kinetics and chemistry are highly desirable.

Over the past decade, laboratory and modeling studies have demonstrated that atmospheric particles

5 can undergo phase separation and exhibit different morphologies, which play a role in many atmospheric processes. For example, the inhomogeneous distribution of inorganic and organic species within phase-separated particles can affect the reactive uptake of gas-phase species (e.g. N_2O_5) (Gaston et al., 2014) and water uptake of organic-inorganic particles (Chan and Chan, 2007; Zuend and Seinfeld, 2012; Hodas et al., 2015). It is still unclear how the occurrence of liquid-liquid phase separation alters

10 the heterogeneous reactivity of organic-inorganic particles over time. As shown in **Figure S2 (***supplementary material***)**, 3-MGA-AS particles become phase separated when the RH is below the SRH (72.7–73.6 %). The phase-separated particles might exhibit different reactivity compared to those in a single liquid phase investigated in this work since the surface composition of the particles are different in these two phases. Furthermore, the phase separation behavior (e.g. SRH) of the particles

15 can change in response to the change in the particle composition during oxidation over time. Although the phase of oxidized 3-MGA-AS particles has not been determined experimentally in this work, the overall ⟨O/C⟩ is found to increase slightly from 0.67 to ~0.75 (*supplementary material*), and the SRH is expected to decrease slightly after oxidation (Bertram et al., 2011; Song et al., 2012b; You et al., 2013, 2014). Since the experimental RH inside the reactor was fixed at 85.0 %, it is very likely that 3-

20 MGA-AS particles remain in a single liquid phase state during oxidation. During oxidation, the degree of aerosol oxidation state (e.g. expressed by ⟨O/C⟩) typically increases due to the formation of more oxygenated reaction products and, consequently, the SRH is expected to decrease. As shown in **Figure 4**, it is hypothesized that initially phase-separated particles might transition to a homogeneous, single liquid phase state, depending on the extent of oxidation and the environmental thermodynamic

25 conditions. Hence, it is of interest to investigate how the phase separation characteristics of organic-inorganic particles change in response to a change in the composition upon oxidation. Moreover, with

respect to future work, it would be interested in understanding the dynamic interplay between the particle composition, heterogeneous reactivity, liquid-liquid phase separation and effects on particle morphology under different environmental conditions and extents of oxidation.

Author contributions

HKL, SMS, and MNC designed and ran the experiments. HKL, SMS, and MNC prepared the manuscript. All co-authors provided comments and suggestions to the manuscript.

Acknowledgements

This work is supported by the Hong Kong Research Grants Council (HKRGC) Project ID: 2191111 (Ref 24300516). We would like to thank Kevin Wilson for his insightful comments.

References

1. Bennett, J. E. and Summers, R.: Product studies of the mutual termination reactions of sec-alkylperoxy radicals: Evidence for non-cyclic termination, Can. J. Chem., 52, 1377–1379, doi:10.1139/v74-209, 1974.

2. Bertram, A. K., Martin, S. T., Hanna, S. J., Smith, M. L., Bodsworth, A., Chen, Q., Kuwata, M., Liu, A., You, Y., and Zorn, S. R.: Predicting the relative humidities of liquid-liquid phase separation, efflorescence, and deliquescence of mixed particles of ammonium sulfate, organic material, and water using the organic-to-sulfate mass ratio of the particle and the oxygen-to-carbon elemental ratio of the organic component, Atmos. Chem. Phys., 11, 10995–11006, 2011.

3. Cappa, C. D., Che, D. L., Kessler, S. H., Kroll, J. H., and Wilson, K. R.: Variations in organic aerosol optical and hygroscopic properties upon heterogeneous OH oxidation, J. Geophys. Res., 116, D15204, 2011.

4. Chan, M. N. and Chan, C. K.: Mass transfer effects on the hygroscopic growth of ammonium sulfate particles with a water-insoluble coating, Atmos. Environ., 41, 4423–4433, 2007.

5. Chan, M. N., Nah, T., and Wilson, K. R.: Real time in-situ chemical characterization of sub-micron organic aerosols using Direct Analysis in Real Time Mass Spectrometry (DART-MS): The effect of aerosol size and volatility, Analyst, 138, 3749–3757, 2013.

6. Chan, M. N., Zhang, H., Goldstein, A. H., and Wilson, K. R.: Role of water and phase in the heterogeneous oxidation of solid and aqueous succinic acid aerosol by hydroxyl radicals, J. Phys. Chem. C, 118, 28978–28992, 2014.

7. Chapleski, Jr. R. C., Zhang, Y., Troyaa, D., and Morris, J. R.: Heterogeneous chemistry and reaction dynamics of the atmospheric oxidants, O_3, NO_3, and OH, on organic surfaces, Chem. Soc. Rev., 45, 3731–3746, 2016.

8. Cheng, C. T., Chan, M. N., and Wilson, K. R.: The role of alkoxy radicals in the heterogeneous reaction of two structural isomers of dimethylsuccinic acid, Phys. Chem. Chem. Phys., 17, 25309–25321, doi:10.1039/c5cp03791c, 2015.

9. Chim, M. M., Chow, C. Y., Davie, J. F., and Chan, M. N.: Effects of relative humidity and particle phase water on the heterogeneous OH oxidation of 2-methylglutaric acid aqueous droplets, J. Phys. Chem. A, 121, 1666–1674, 2017a.

10. Chim, M. M., Cheng C. T., Davies, J. F., Berkemeier, T., Shiraiwa, M., Zuend, A., and Chan, M. N.: Compositional evolution of particle-phase reaction products and water in the heterogeneous OH oxidation of model aqueous organic aerosols, Atmos. Chem. Phys., 17, 14415–14431, 2017b.

11. Ciobanu, V. G., Marcolli, C., Krieger, U. K., Weers, U., and Peter, T.: Liquid-liquid phase separation in mixed organic/inorganic aerosol particles, J. Phys. Chem. A, 113, 10966–10978, 2009.

12. Cody, R. B.: Observation of molecular ions and analysis of nonpolar compounds with the direct analysis in real time ion source, Anal. Chem., 81, 1101−1107, 2009.

13. Cody, R. B., Laramée, J. A., and Durst, H. D., Versatile new ion source for the analysis of materials in open air under ambient conditions, Anal. Chem., 77, 2297−2302, 2005.

14. Davies, J. F. and Wilson, K. R.: Nanoscale interfacial gradients formed by the reactive uptake of OH radicals onto viscous aerosol surfaces, Chem. Sci., 6, 7020−7027, 2015.

15. Dennis-Smither, B. J., Miles, R. E. H., and Reid, J. P.: Oxidative aging of mixed oleic acid/sodium chloride aerosol particles, J. Geophys. Res., 117, D20204, doi:10.1029/ 2012JD018163, 2012.

16. Estillore, A. D., Trueblood, J. V., and Grassian, V. H.: Atmospheric chemistry of bioaerosols: Heterogeneous and multiphase reactions with atmospheric oxidants and other trace gases, Chem. Sci. 7 (11), 6604−6616, 2016.

17. Fan, H., Tinsley, M. R., and Goulay, F.: Effect of relative humidity on the OH-initiated heterogeneous oxidation of monosaccharide nanoparticles, J. Phys. Chem. A, 119(45), 11182–11190, 2015.

18. Freedman, M. A.: Phase separation in organic aerosol, Chem. Soc. Rev., 46, 7694–7705, 2017.

19. Gaston, C. J., Thornton, J. A., and Ng, N. L.: Reactive uptake of N_2O_5 to internally mixed inorganic and organic particles: the role of organic carbon oxidation state and inferred organic phase separations, Atmos. Chem. Phys., 14, 5693–5707, 2014.

20. George, I. J., Vlasenko, A., Slowik, J. G., Broekhuizen, K., and Abbatt, J. P. D.: Heterogeneous oxidation of saturated organic aerosols by hydroxyl radicals: uptake kinetics, condensed-phase products, and particle size change, Atmos. Chem. Phys., 7, 4187–4201, 2007.

21. George, I. J. and Abbatt, J. P. D.: Heterogeneous oxidation of atmospheric aerosol particles by gas-phase radicals, Nature Chem., 2, 713−722, 2010.

22. Hajslova, J., Cajka, T., and Vaclavik, L.: Challenging applications offered by direct analysis in real time (DART) in food-quality and safety analysis, TrAC Trend. Anal. Chem., 30, 204−218, 2011.

23. Hodas, N., Zuend, A., Mui, W., Flagan, R. C., and Seinfeld, J. H.: Influence of particle-phase state on the hygroscopic behavior of mixed organic-inorganic aerosols, Atmos. Chem. Phys., 15, 5027–5045, 2015.

24. Jimenez, J., Canagaratna, M., Donahue, N., Prevot, A., Zhang, Q., Kroll, J. H., DeCarlo, P. F., Allan, J. D., Coe, H., and Ng, N.: Evolution of organic aerosols in the atmosphere, Science, 326, 1525−1529, 2009.

25. Kanakidou, M., Seinfeld, J. H., Pandis, S. N., Barnes, I., Dentener, F. J., Facchini, M. C., Dingenen, R. V., Ervens, B., Nenes, A. N. C. J. S. E., Nielsen, C. J., and Swietlicki, E.: Organic aerosol and global climate modelling: a review, Atmos. Chem. Phys., 5, 1053–1123, 2005.

26. Kroll, J. H., Lim, C. Y., Kessler, S. H., and Wilson, K. R.: Heterogeneous oxidation of atmospheric organic aerosol: Kinetics of changes to the amount and oxidation of particle-phase organic carbon, J. Phys. Chem. A, 119, 10767–10783, 2015.

27. Kwong, K. C., Chim, M. M., Davies, J. F., Wilson, K. R., and Chan, M. N.: Importance of sulfate radical anion formation and chemistry in heterogeneous OH oxidation of sodium methyl sulfate, the smallest organosulfate, Atmos. Chem. Phys., 18, 2809–2820, doi:10.5194/acp-18-2809-2018, 2018a.

28. Kwong, K. C., Chim, M. M., Hoffmann, E. H., Tilgner, A., Herrmann, H., Davies, J. F., Wilson, K. R., and Chan, M. N.: Chemical transformation of methanesulfonic acid and sodium methanesulfonate through heterogeneous OH oxidation, ACS Earth Space Chem., 2, 895–903 2018b.

29. Lambe, A. T., Zhang, J. Y., Sage, A. M., and Donahue, N. M.: Controlled OH radical production via ozone-alkene reactions for use in aerosol aging studies, Environ. Sci. Technol., 41, 2357–2363, 2007.

30. Lambe, A. T., Miracolo, M. A., Hennigan, C. J., Robinson, A. L., and Donahue, N. M.: Effective rate constants and uptake coefficients for the reactions of organic molecular markers (n-alkanes, hopanes, and steranes) in motor oil and diesel primary organic aerosols with hydroxyl radicals, Environ. Sci. Technol., 43, 8794–8800, 2009.

31. Li, Z., Smith, K. A., and Cappa, C. D.: Influence of relative humidity on the heterogeneous oxidation of secondary organic aerosol, Atmos. Chem. Phys., 18, 14585–14608, 2018.

32. Losey, D. J., Ott, E. J. E., and Freedman, M. A.: Effects of high acidity on phase transitions of an organic aerosol, J. Phys. Chem. A, 122(15), 3819–3828, 2018.

33. Marshall, F. H., Berkemeier, T., Shiraiwa, M., Nandy, L., Ohm, P. B., Dutcher, C. S., and Reid, J. P.: Influence of particle viscosity on mass transfer and heterogeneous ozonolysis kinetics in aqueous-sucrose-maleic acid aerosol, Phys. Chem. Chem. Phys., 20, 11560–11573, 2018.

34. McNeill, V. F., Wolfe, G. M., and Thornton, J. A.: The oxidation of oleate in submicron aqueous salt aerosols: Evidence of a surface process, J. Phys. Chem. A, 111, 1073–1083, 2007.

35. McNeill, V. F., Yatavelli, R. L. N., Thornton, J. A., Stipe, C. B., and Landgrebe, O.: Heterogeneous OH oxidation of palmitic acid in single component and internally mixed aerosol particles: vaporization and the role of particle phase, Atmos. Chem. Phys., 8, 5465–5476, 2008.

36. Mungall, E. L., Wong, J. P. S., and Abbatt, J. P. D.: Heterogeneous Oxidation of Particulate Methanesulfonic Acid by the Hydroxyl Radical: Kinetics and Atmospheric Implications, ACS Earth Space Chem., 2, 48−55, 2017.

37. Nah, T., Chan, M. N., Leone, S. R., and Wilson, K. R.: Real time in situ chemical characterization of submicrometer organic particles using direct analysis in real time-mass spectrometry, Anal. Chem., 85, 2087–2095, 2013.

38. Peeters, J., Fantechi, G., and Vereecken, L.: A generalized structure-activity relationship for the decomposition of (substituted) alkoxy radicals, J. Atmos. Chem., 48, 59–80,2004.

39. Qiu, Y. and Molinero, V.: Morphology of liquid-liquid phase separated aerosols, J. Am. Chem. Soc., 137, 10642–10651, doi:1021/jacs.5b05579, 2015.

40. Reid, J. P., Dennis-Smither, B. J., Kwamena, N. O. A., Miles, R. E. H., Hanford, K. L., and Homer, C. J.: The morphology of aerosol particles consisting of hydrophobic and hydrophilic phases, hydrocarbons. alcohols and fatty acids as the hydrophobic component, Phys. Chem. Chem. Phys., 13, 15559–15572, 2011.

41. Renbaum, L. H. and Smith, G. D.: The importance of phase in the radical-initiated oxidation of model organic aerosols: Reactions of solid and liquid brassidic acid particles, Phys. Chem. Chem. Phys., 11, 2441−2451, 2009.

42. Richards-Henderson, N. K., Goldstein, A. H., and Wilson, K. R.: Large enhancement in the heterogeneous oxidation rate of organic aerosols by hydroxyl radicals in the presence of nitric oxide, J. Phys. Chem. Lett., 6(22), 4451–4455, 2015.

43. Rudich, Y., Donahue, N. M., and Mentel, T. F.: Aging of organic aerosol: bridging the gap between laboratory and field studies, Annu. Rev. Rhys. Chem., 58, 321–352, 2007.

44. Russell, G. A.: Deuterium-isotope effects in the autoxidation of aralkyl hydrocarbons. mechanism of the interaction of peroxy radicals, J. Am. Chem. Soc., 79, 3871–3877, doi:10.1021/ja01571a068, 1957.

45. Shiraiwa, M., Ammann, M., Koop, T., and Pöschl, U.: Gas uptake and chemical aging of semisolid organic aerosol particles, Proc. Natl. Acad. Sci., 108(27), 11003–11008, 2011.

46. Slade, J. H. and Knopf, D. A.: Heterogeneous OH oxidation of biomass burning organic aerosol surrogate compounds: Assessment of volatilization products and the role of OH concentration on the reactive uptake kinetics, Phys. Chem. Chem. Phys., 15, 5898–5915, 2013.

47. Slade, J. H. and Knopf, D. A.: Multiphase OH oxidation kinetics of organic aerosol: The role of particle phase state and relative humidity, Geophys. Res. Lett., 41(14), 5297–5306, 2014.

48. Smith, J. D., Kroll, J. H., Cappa, C. D., Che, D. L., Liu, C. L., Ahmed, M., Leone, S. R., Worsnop, D. R., and Wilson, K. R.: The heterogeneous reaction of hydroxyl radicals with sub-micron squalane particles: a model system for understanding the oxidative aging of ambient aerosols, Atmos. Chem. Phys., 9, 3209–3222, doi:10.5194/acp-9-3209-2009, 2009.

49. Song, M., Marcolli, C., Krieger, U. K., Zuend, A., and Peter, T.: Liquid-liquid phase separation and morphology of internally mixed dicarboxylic acids/ammonium sulfate/water particles, Atmos. Chem. Phys., 12, 2691–2712, 2012a.

50. Song, M., Marcolli, C., Krieger, U. K., Zuend, A., and Peter, T.: Liquid-liquid phase separation in aerosol particles: Dependence on O:C, organic functionalities, and compositional complexity, Geophys. Res. Lett., 39, L19801, 2012b.
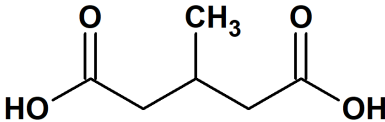
51. Song, M. J., Marcolli, C., Krieger, U. K., Zuend, A., and Peter, T.: Morphologies of mixed organic/inorganic/aqueous aerosol droplets, Faraday Discuss., 165, 289–316, 2013.

52. Stewart, D. J., Cai, C., Nayler, J., Preston, T. C., Reid, J. P., Krieger, U. K., Marcolli, C., and Zhang, Y. H.: Liquid-liquid phase separation in mixed organic/inorganic single aqueous aerosol droplets, J. Phys. Chem. A, 119, 4177–4190, 2015.

53. Vereecken L. and Peeters, J.: Decomposition of substituted alkoxy radicals – Part I: A generalized structure-activity relationship for research barrier heights, Phys. Chem. Chem. Phys., 11, 9062–9074, 2009.

54. You, Y. and Bertram, A. K.: Effect of molecular weight and temperature on liquid-liquid phase separation in particles containing organic species and inorganic salts, Atmos. Chem. Phys., 15, 1351–1365, 2015.

55. Zhang, Q., Jimenez, J. L., Canagaratna, M. R., Allan, J. D., Coe, H., Ulbrich, I., Alfarra, M. R., Takami, A., Middlebrook, A. M., Sun, Y. L., Dzepina, K., Dunlea, E., Docherty, K., DeCarlo, P. F., Salcedo, D., Onasch, T., Jayne, J. T., Miyoshi, T., Shimono, A., Hatakeyama, S., Takegawa, N., Kondo, Y., Schneider, J., Drewnick, F., Borrmann, S., Weimer, S., Demerjian, K., Williams, P., Bower, K., Bahreini, R., Cottrell, L., Griffin, R. J., Rautiainen, J., Sun, J. Y., Zhang, Y. M., and Worsnop, D. R.: Ubiquity and dominance of oxygenated species in organic aerosols in anthropogenically-influenced Northern Hemisphere midlatitudes, Geophys. Res. Lett., 34, L13801, 2007.

56. Zuend, A. and Seinfeld, J. H.: Modeling the gas-particle partitioning of secondary organic aerosol: The importance of liquid-liquid phase separation, Atmos. Chem. Phys., 12, 3857–3882, 2012.

57. Zuend, A., Marcolli, C., Luo, B. P., and Peter, T.: A thermodynamic model of mixed organic-inorganic aerosols to predict activity coefficients, Atmos. Chem. Phys., 8, 4559–4593, 2008.

58. Zuend, A., Marcolli, C., Booth, A. M., Lienhard, D. M., Soonsin, V., Krieger, U. K., Topping, D. O., McFiggans, G., Peter, T., and Seinfeld, J. H.: New and extended parametrization of the thermodynamic model AIOMFAC: Calculation of activity coefficients for organic-inorganic

mixtures containing carboxyl, hydroxyl, carbonyl, ether, ester, alkenyl, alkyl, and aromatic

functional groups, Atmos. Chem. Phys., 11, 9155–9206, 2011.

Table 1. Chemical structure, properties, effective heterogeneous OH rate constant, effective OH uptake coefficient of 3-methylglutaric acid (3-MGA) and 3-MGA mixed with ammonium sulfate (AS) in an organic-to-inorganic dry mass ratio (OIR) = 2.

Chemical structure		
Chemical formula	$C_6H_{10}O_4$	
O/C ratio	0.67	
H/C ratio	1.67	
	3-MGA	**3-MGA-AS** (OIR =2)
Separation RH (SRH)	–	72.7–73.6 %
Mass fraction at 85 % RH		
3-MGA	0.707	0.344
AS	0	0.172
H_2O	0.293	0.484
Effective second order heterogeneous OH rate constant, k ($\times 10^{-12}$ cm^3 molecule^{-1} s^{-1})	3.26 ± 0.065	2.72 ± 0.064
Effective OH uptake coefficient, γ_{eff}	2.41 ± 0.13	0.99 ± 0.05
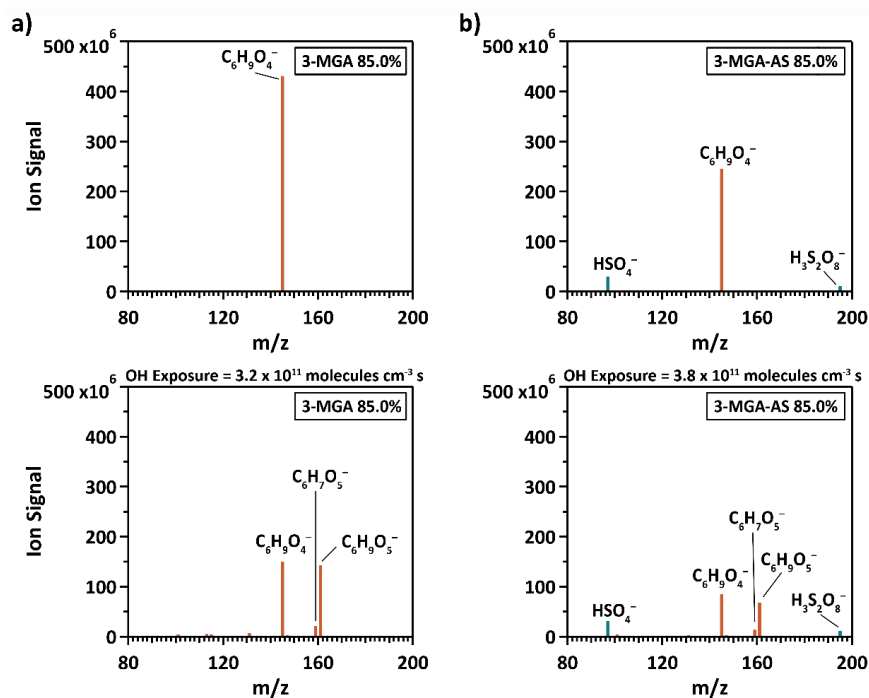
Figure 1. The particle mass spectrum of a) 3-MGA and b) 3-MGA-AS before (upper panels) and after (lower panels) heterogeneous OH oxidation at 85.0 % RH, respectively. Color scheme: brown = organic species, blue = inorganic species.
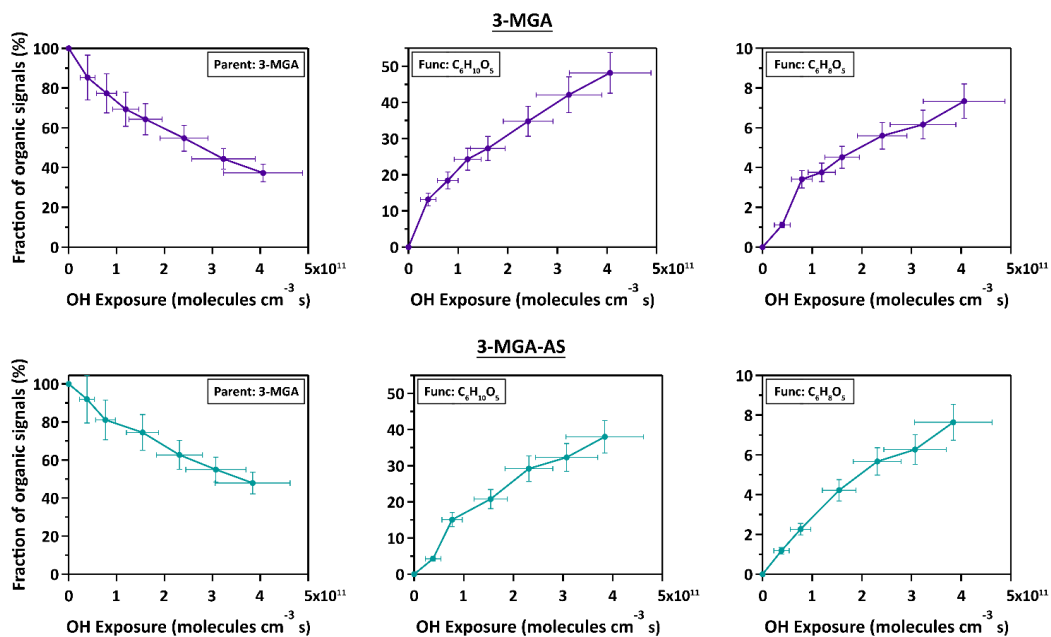
Figure 2. Upper panels: The fraction of the organic ion signal attributed to the parent 3-MGA, the major C_6 hydroxyl and C_6 ketone products of 3-MGA particles during the heterogeneous OH oxidation shown against OH exposure. Lower panels: analogous to the above, but for the case of mixed 3-MGA-AS particles.
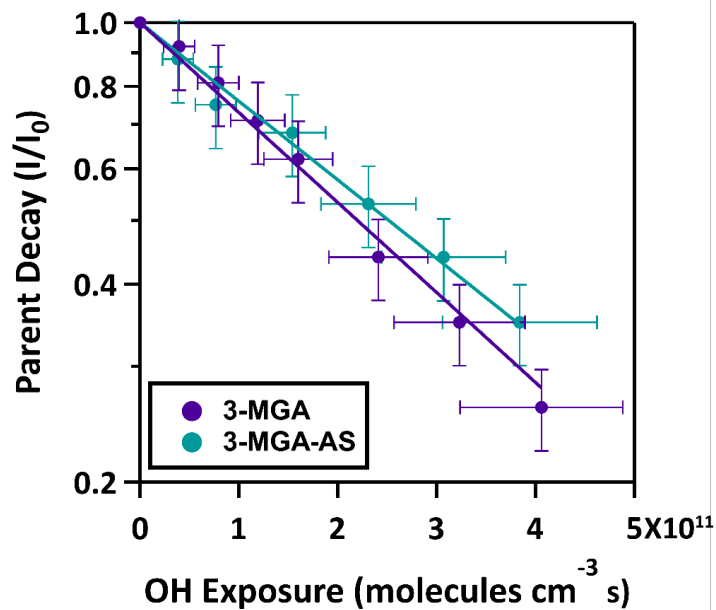
Figure 3. The normalized parent decay for the heterogeneous OH oxidation of 3-MGA and 3-MGA-

AS particles at 85.0 % RH. Note the logarithmic scale of the ordinate.
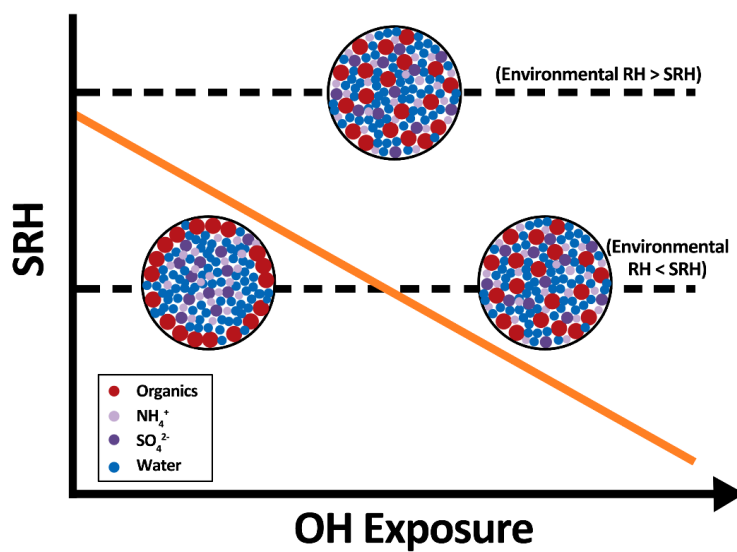
Figure 4. A simplified diagram illustrating the change in separation relative humidity (SRH, orange solid line) and phase composition of droplets containing inorganic salts and organic compounds (single liquid phase vs. liquid-liquid phase separated) upon heterogeneous oxidation at two different environmental RH.
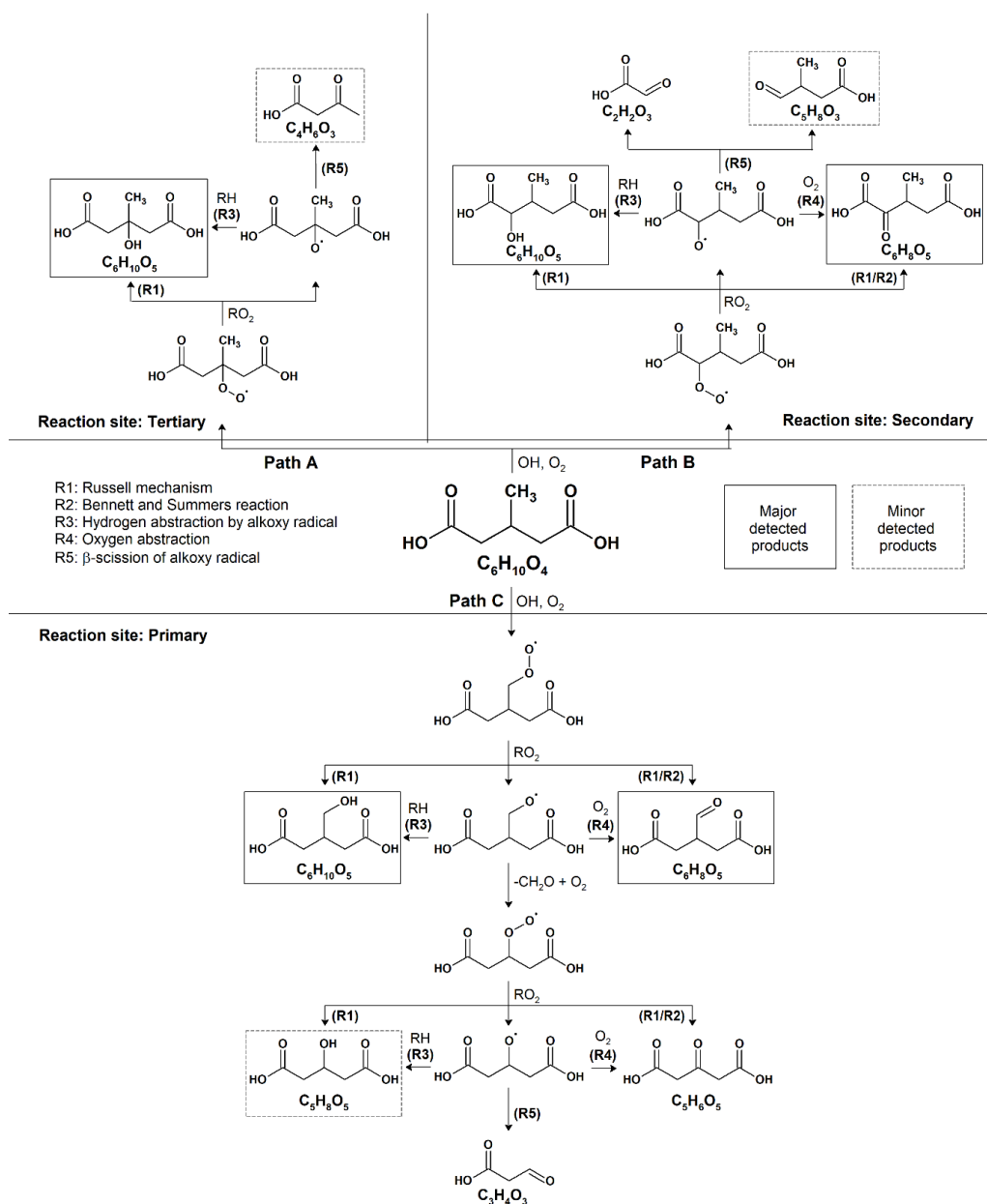
Scheme 1. Proposed reaction mechanisms for the heterogeneous OH oxidation of 3-MGA and 3-MGA-AS particles.

TOC.